Free-surface dynamics in the Ribbon Growth on Substrate (RGS) process

P Beckstein, V Galindo, G Gerbeth, A Schönecker

Free-surface dynamics in the Ribbon Growth on Substrate (RGS) process

P.Beckstein[1], V. Galindo[1], G. Gerbeth[1], A. Schönecker[2]

[1]Helmholtz-Zentrum Dresden-Rossendorf, Bautzner Landstr. 400, 01328 Dresden, Germany
[2]RGS Development B.V., Bijlestaal 54A, 1721 Broek op Langedijk, The Netherlands

Corresponding author: p.beckstein@hzdr.de

Abstract

The cost efficient, high throughput production of metal- and semiconductor alloys is the foundation of many advanced technologies. With the development of the Ribbon Growth on Substrate (RGS) technology, a new crystallization technique is available that allows the controlled, high crystallization rate production of silicon wafers and advanced metal-silicide alloys. Compared to other crystallization methods, such as melt spinning, the RGS process allows better crystallization control, high volume manufacturing and high material yield due to the substrate driven process. In order to optimize RGS further, insights from modelling the liquid metal in the casting frame under electromagnetic fields are very desirable. We performed numerical investigations in order to study the involved AC magnetic fields, which are an essential part of the RGS process to realize a magnetic retention effect. Our simulation results demonstrate the effect of the applied AC magnetic fields on the silicon melt flow. The main focus is thereby devoted to the simulation of the melt surface deformation based on a complex modelling approach. This time-dependent free-surface flow under the influence of magnetic forces is the key for optimizing the RGS process.

Key words: Ribbon Growth on Substrate, Semi-conductor processing, AC magnetic fields, Magnetic retention, OpenFOAM extensions, COMSOL Multiphysics, Moving mesh, Surface-tracking, Free-surface, Dome-shaping

Introduction

The basic idea of the RGS process [1, 2] for the production of silicon wafers is a continuous feeding of molten silicon into a bottomless casting frame, while a solidified silicon foil is extracted sidewise on a sub-cooled moving substrate underneath. Fig. 1 depicts this principle. The sketch represents one half of the core process viewing towards a central cutting section.

The AC magnetic fields which are used for inductive heating bear a two-fold meaning. That is, a single excitation coil provides both heat and a kind of magnetic valve. The latter actively prevents leakage in the slit regions and reduces oscillations at the extraction site of the silicon foil through electromagnetic forces. This Lorentz force field is acting to counter the gravitational forces on the melt, which only works in conjunction with surface tension.

We demonstrate the effect of the applied AC magnetic fields on the silicon melt in the RGS process, taking into account the time-dependent coupling to the flow in the melt.

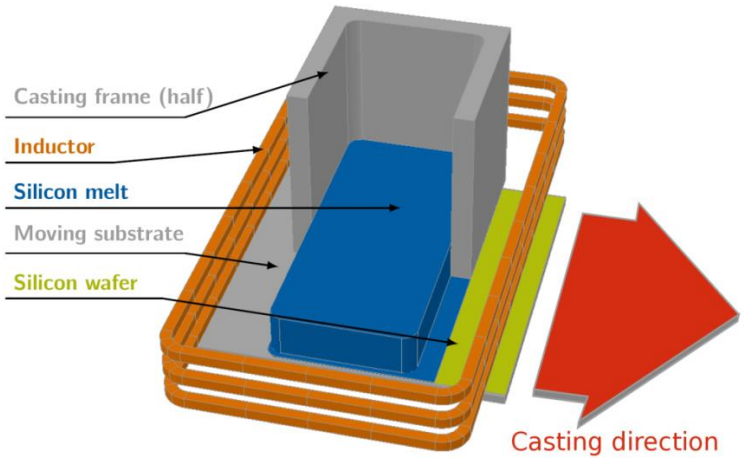

Fig. 1: Scheme of the RGS process with excitation coils [1].

Numerical Model

The casting region in the real RGS prototype machine [1] is a complex and detailed system. Therefore, a simplified set of modeling parameters and casting environment geometry was derived. It is expected that this numerical model allows the calculation of the main effects of the liquid silicon behavior and its results should still allow a comparison to real process data from the RGS process. For this simplified model the RGS wafer size is given by $156\,mm \times 156\,mm \times 0.4\,mm$. The mean melt level height inside the casting frame is assumed to be $h = 20\,mm$, the length of the melt region in process direction is $l = 70\,mm$ and the width $w = 150\,mm$. A typical set of process parameters, which evolved mainly from empirical analysis, is a RMS-current of $I_{RMS} = 1000$ A at a frequency of $f = 10$ kHz to feed the excitation coils in combination with a substrate velocity of $u_S = 0.1\,\mathrm{m/s}$ in process direction. The most important properties of materials shown in Fig. 1 are listed in Table 1.

Material	ρ [kg/m^3]	η [Pa · s]	σ [S/m]	γ [N/m] (Air)	δ [mm]
Liquid silicon	2580	0.86 x 10^{-3}	1.20 x 10^6	0.733	5.0
Solid silicon	2330	-	8.30 x 10^4	-	17.0
Graphite (casting frame)	1880	-	1.25 x 10^5	-	14.0
Copper (inductor)	8960	-	6.00 x 10^7	-	0.7

Table 1: Material properties for different materials: Density ρ, kinematic viscosity η, electrical conductivity σ, surface tension γ and skin depth $\delta = \sqrt{1/(\pi f \mu_0 \sigma)}$ for a frequency of $f = 10\ kHz$.

The physical description of the magnetic fields in our model is based on the $\boldsymbol{A}$-V-formulation of the quasi-static Maxwell-Equations with implied MHD approximations. In addition, assuming only a very small magnetic Reynolds number and neglecting magnetization effects is valid for our purposes with sufficient quality. Introducing the velocity field $\boldsymbol{u}$ and the physical time t we may summarize these assumptions as follows:

$$\boldsymbol{B} = \boldsymbol{\nabla} \times \boldsymbol{A}\,; \quad \boldsymbol{E} = -(\partial_t \boldsymbol{A} + \boldsymbol{\nabla} V)\,; \quad \|\boldsymbol{u} \times \boldsymbol{B}\| / \|\boldsymbol{E}\| \ll 1\,. \tag{1}$$

Using the magnetic vector potential $\boldsymbol{A}$ with applied Coulomb-Gauge ($\nabla \cdot \boldsymbol{A} = \boldsymbol{0}$) and the electric scalar potential V to describe the magnetic $\boldsymbol{B}$ and electric field $\boldsymbol{E}$ allows us to explicitly introduce a source current density $\boldsymbol{j}_{\mathrm{E}}(I_{RMS})$ term into the system which represents the effect of the excitation coil [3, 4]. For constant electrical conductivity the scalar potential may be incorporated into a modified magnetic vector potential according to $\widehat{\boldsymbol{A}} = \boldsymbol{A} + \int \boldsymbol{\nabla} V \mathrm{d}t$ [5]:

$$\boldsymbol{\nabla} \times \boldsymbol{\nabla} \times \widehat{\boldsymbol{A}} + \sigma \mu_0\, \partial_t \widehat{\boldsymbol{A}} = \mu_0 \boldsymbol{j}_{\mathrm{E}}\,; \quad \boldsymbol{j} = \boldsymbol{j}_{\mathrm{I}} + \boldsymbol{j}_{\mathrm{E}}\,; \quad \boldsymbol{j}_{\mathrm{I}} = -\sigma\, \partial_t \widehat{\boldsymbol{A}}\,. \tag{2}$$

The field $\boldsymbol{j}_I$ represents the purely induced current density. To apply suitable boundary conditions, the numerical domain is divided into several regions with constant σ. A detailed mathematical description of all boundary/transition conditions can be found in [3]. By introducing complex-valued sinusoidal fields, equation (2) can be transformed into the complex domain for an angular frequency of $\omega = 2\pi f$. This approach leads to a quasi-stationary problem. For the momentum balance of the fluid, only the time-averaged Lorentz force $\boldsymbol{F_L} = 1/\rho \langle \boldsymbol{j} \times \boldsymbol{B} \rangle_{\mathrm{t}}$ is important. Supposing a negligible influence of natural convection, the fluid dynamics of the liquid melt (cf. Fig. 1) are governed by the principle of conservation of mass and momentum in form of the incompressible, isothermal Navier-Stokes-Equation [6] for a Newtonian fluid with additional terms for gravity and the time-averaged Lorentz-Force as described above:

$$\rho[\partial_t \boldsymbol{u} + (\boldsymbol{u} \cdot \boldsymbol{\nabla})\boldsymbol{u}] = \boldsymbol{\nabla} \cdot \boldsymbol{\tau} + \rho \boldsymbol{g} + \boldsymbol{F}_L; \quad \boldsymbol{\nabla} \cdot \boldsymbol{u} = 0\,; \tag{3}$$

$$\boldsymbol{\tau} = \eta[\boldsymbol{\nabla u} + (\boldsymbol{\nabla u})^T] - p\boldsymbol{I}\,. \tag{4}$$

Here $\boldsymbol{\tau}$ represents the total stress tensor including the diagonal fluid pressure p. For our model only the fluid flow in the bulk region (cf. Fig. 1) is considered. The corresponding numerical domain is hence bounded by the top free-surface, stationary side walls and the liquid/solid interface (cf. Fig. 1). The latter is assumed to be planar and being translated with the casting velocity $\boldsymbol{u}_S$ of the moving substrate.

Surface tension is acting on the free-surface boundary. To keep our model simple, it is assumed to be constant and given by a constant coefficient γ. It is thereby worth to mention that the viscosity of the external atmosphere, which is in contact with the liquid melt at the free-surface, is several orders of magnitude smaller than the viscosity of the melt itself. Thus, the fluid boundary condition at the free-surface can be modeled using a simplified Young-Laplace-Equation [7] neglecting tangential drag forces from the atmosphere. Stationary walls are modelled with no-slip boundary conditions, whereas for the bottom wall of the fluid domain an inhomogeneous Dirichlet boundary condition is applied to simulate the substrate movement.

The free-surface movement and flow calculation is represented by means of a three-dimensional finite-volume surface tracking method based on *OpenFOAM* [8] with a dynamic moving mesh [7, 9]. This utilized approach is known as Arbitrary Lagrangian-Eulerian formulation (ALE). In simplified terms, the essential idea of ALE is to allow the grid - which is used for discretization - to move independently from the fluid flow, except for the domain boundaries. The free-surface is under constraint, such that the fluid velocity equals the mesh velocity $\boldsymbol{u}_M$ in normal direction there. For all other boundaries $\boldsymbol{u}_{\mathrm{M}}$ is restricted according to the meaning of the boundary for the mesh (e.g. slip/no-slip). The independent mesh-movement away from the boundaries allows a free and preferably smooth mesh point distribution. In our case a Laplace-smoothing for $\boldsymbol{u}_{\mathrm{m}}$ was utilized [10]. In the sense of ALE, equations (2) and (3) have to be considered as relative to the mesh motion $\boldsymbol{u}_{\mathrm{m}}$ in a Lagrangian manner.

In order to realize the coupling of the magnetodynamic and hydrodynamic effects, a combination of a modified solver of *OpenFOAM extensions* [11] and the finite-element software *COMSOL Multiphysics* [12] is used. The Lorentz force calculation with interpolated free-surface location-data is achieved with *COMSOL Multiphysics* which is iteratively

coupled to *OpenFOAM* for the flow calculation with interpolated Lorentz force data. The backend-scripting for automation, interpolation and smoothing is written in *Python* and *PyFoam*. The surface-tracking approach on a moving computational domain allows us to "carry" the Lorentz force distribution $\boldsymbol{F}_L$ with the mesh for a defined and reasonable small simulation time, which allows us to greatly improve the overall performance.

Simulation results

Previous studies [13, 14] provided an overview of magnetohydrodynamic effects in the RGS process at its characteristic process parameters as given above. We have already successfully performed 3D-simulations with fixed melt geometry to numerically confirm the functioning melt retention based on magnetic fields. It has been illustrated that a retention effect is correlated with a strong forced fluid flow. A parameter study revealed the total system inductivity as a function of the melt level, which might be usable for a fill-level sensing of the silicon melt. In particular, we also demonstrated that the surface deformation is substantially important for a satisfactory model. The Lorentz force acting on a conducting liquid inside a coil is roughly pointing towards the center of this coil. Consequently, the shape of the deformed fluid domain for these and similar cases looks similar to a dome. This process is often referred to as "dome shaping" [4]. For the RGS process parameters we revealed that the influence of the Lorentz force on the fluid flow is much more intense than the drag force from the moving substrate wall.

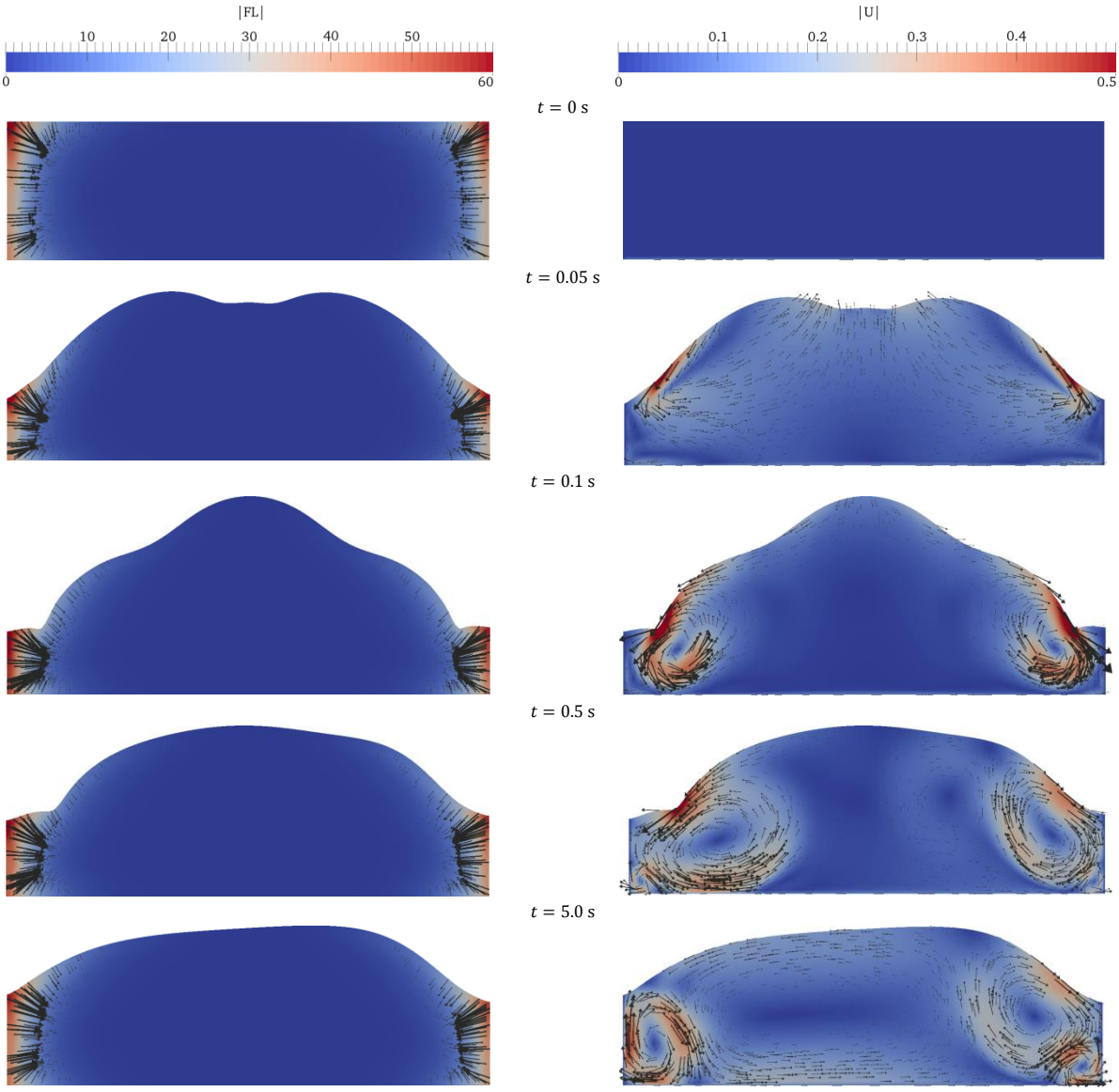

Fig. 2: Evolution of the free-surface flow at the central section of the fluid domain with its dome-shape after applying the magnetic field for a constant surface level at $t = 0\ s$ (left: $\boldsymbol{F}_L/\rho[m/s^2]$; right: $\|\boldsymbol{u}\|\ [m/s]$). The Lorentz force was updated every $\Delta t = 0.01\ s$.

Due to the challenging numerical conditions, several numerical tests were necessary in order to ensure stability of our modified *OpenFOAM*-solver. In the frame of this investigation we had to optimize our selection of finite-volume discretization schemes to account for possible high mesh skewness and a bounded solution, implement an automatic time step control, introduce a volume correction algorithm to obey mass conservation, improve parts of the surface-tracking procedure and fix bugs in *OpenFOAM extensions*. To increase solver performance and to allow unsteady RANS-simulations on coarse meshes, the usage of the class for turbulence and sub-grid-scale-models of *OpenFOAM* has been implemented in our solver, too. The k-ω-SST turbulence model [15] was applied for all flow simulations.

As a proof of concept, Fig. 2 shows a time-series of the free-surface flow at the central section of the fluid domain with its evolving dome-shape. The magnetic field was applied at $t = 0\ s$ for a constant surface level of $h = 20\ mm$ (Process direction is widthwise from left to right). In the left column one can comprehend how the Lorentz force density $\boldsymbol{F}_L/\rho[m/s^2]$ is changing during time. The right hand side illustrates the corresponding velocity magnitude $\|\boldsymbol{u}\|\ [m/s]$ and flow direction. For this calculation, the Lorentz force was updated every $\Delta t_L = 0.01\ s$. Since the magnetic vector potential as given by equation (2) is calculated for the whole simplified model (cf. Fig. 1) including casting frame, substrate and wafer, the result is not symmetric. This asymmetry is obvious for advanced time instances ($t > 0.5\ s$). Even though one could spuriously hold the moving substrate wall at the bottom responsible for the large developing vortex flow in the central part, it is mainly induced by the asymmetric Lorentz force distribution.

Conclusion

The RGS process is a promising technology for the production of silicon wafers and advanced metal-silicide alloys. In order to optimize RGS, it is desired to deliver a better insight into the free-surface dynamics. We have developed a new solver concept to model the flow of conducting fluids under the influence of AC magnetic fields. On this basis we have successfully conducted unsteady simulations of the free-surface dynamics under typical conditions of the RGS process. There are still a number of remaining problems to be addressed, especially for large 3D-simulations concerning numerical stability. This is subject of our current and future investigation. To validate our newly developed code, future work will be devoted to prepare different experimental test cases as a basis for quantitative comparison in the following step. There is also much room for improvement regarding the overall performance of the solution algorithm. Although we have already put much effort in reducing computational overhead due to the coupling of *OpenFOAM* and *COMSOL Multiphysics* to a minimum, it cannot be avoided completely with our current implementation. In this regard, we will develop a concept for assessing the feasibility of solving the partial differential equation (3) for the magnetic vector potential in *OpenFOAM*, too. This would allow us to solve all physics in just one framework.

Acknowledgements

Financial support for this research from the German Helmholtz Association in frame of the Alliance “Liquid Metal Technologies (LIMTECH)” is gratefully acknowledged. We would also like to thank our colleagues from “RGS Development B.V.” for all their generous support and lively discussions.

References

[1] A. Schönecker, L. J. Geerligs and A. Müller (2004), Solid State Phenomena 95-96, 149-158

[2] G. Hahn and A. Schönecker (2004), Journal of Physics: Condensed Matter 16, R1615-R1648

[3] K. J. Binns, P. J. Lawrenson and C. W. Trowbridge (1992), The Analytical and Numerical Solution of Electric and Magnetic Fields, Wiley

[4] R. Moreau (1990), Magnetohydrodynamics, Kluwer

[5] T. Morisue (1982), IEEE Transactions on Magnetics 18, 531-535

[6] J. H. Ferziger and M. Peric (2002), Computational Methods for Fluid Dynamics, Springer

[7] R. Scardovell and S. Zalesk (1999), Annual Review of Fluid Mechanics 31, 567-603

[8] H. Weller, G. Tabor, H. Jasak and C. Fureby (1998), Computational Physics 12-6, 620-631

[9] H. Jasak (2009), 47th AIAA Aerospace Sciences Meeting Including The New Horizons Forum and Aerospace Exposition, Orlando

[10] H. Jasak and Z. Tukovic (2007), Transactions of FAMENA

[11] Z. Tukovic and H. Jasak (2012), Computers & Fluids 55, 70-84

[12] COMSOL Multiphysics 4.4 (2014), Reference Manual

[13] P. Beckstein, V. Galindo and G. Gerbeth (2014), Proceedings of the 9th International PAMIR Conference on Fundamental and Applied MHD 2, 196-201

[14] P. Beckstein, V. Galindo and G. Gerbeth (2015), Magnetohydrodynamics, in press

[15] F. R. Menter (1994), AIAA Journal 32-8, 1598-1605